



Highly efficient and noble metal-free NiS modified $Mn_xCd_{1-x}S$ solid solutions with enhanced photocatalytic activity for hydrogen evolution under visible light irradiation

Xiaolei Liu^a, Xizhuang Liang^a, Peng Wang^{a,*}, Baibiao Huang^{a,*}, Xiaoyan Qin^a, Xiaoyang Zhang^a, Ying Dai^b

^a State Key Laboratory of Crystal Materials, Shandong University, Jinan 250100, China

^b School of Physics, Shandong University, Jinan 250100, China

ARTICLE INFO

Article history:

Received 18 August 2016

Received in revised form 12 October 2016

Accepted 14 October 2016

Available online 17 October 2016

Keywords:

High efficient

Noble metal-free

Photocatalytic hydrogen evolution

NiS modified $Mn_xCd_{1-x}S$ nanocomposites
In situ

ABSTRACT

In this work, a series of highly efficient and noble metal-free NiS modified $Mn_xCd_{1-x}S$ nanocomposites were synthesized via a simple direct in situ precipitation process. The as-synthesized products were characterized by XRD, UV-vis DRS, SEM, EDS, TEM, HRTEM, XPS, PL and TRFIA (the time resolved fluorescence spectra). Hydrogen evolution of as-synthesized NiS/ $Mn_xCd_{1-x}S$ composites in the presence of $Na_2S-Na_2SO_3$ under visible light irradiation ($\lambda \geq 420$ nm) was investigated. The results demonstrated that photocatalytic hydrogen evolution of $Mn_{0.5}Cd_{0.5}S$ was significantly enhanced by loading NiS nanoparticles. As a highly efficient co-catalyst, the optimal NiS loading content was found to be 0.3 wt%, giving a H_2 evolution rate of 419.3 $\mu\text{mol}/\text{h}$ with an apparent quantum efficiency (QE) of 5.21% (420 nm), which was nearly 18.6 and 3.1 times than that of $Mn_{0.5}Cd_{0.5}S$ and 1.0 wt% Pt/ $Mn_{0.5}Cd_{0.5}S$ under the same condition. This work reveals that low cost and earth-abundant NiS can replace noble metals as a highly efficient co-catalyst in hydrogen evolution.

© 2016 Elsevier B.V. All rights reserved.

1. Introduction

Excessive consumption of fossil fuels and the pollution associated with fossil fuels combustion have driven human society to explore environmental friendly and renewable energy resources. Hydrogen (H_2) energy as an ideal candidate has received much attention owing to environmental friendliness, high-energy capacity and recycling possibility [1,2]. Semiconductor photocatalytic water splitting has been considered as a promising and attractive way to convert freely available solar energy into hydrogen energy since first discovery of this process on titania electrodes by Honda and Fujishima in 1972 [3]. During the past few decades, many photocatalytic materials have been developed to produce hydrogen by solar energy driven water splitting such as sulfide-, oxide- and oxynitride based materials [4–8]. Among various semiconductor photocatalysts, sulfide-based materials are regarded as good candidates for hydrogen evolution owing to suitable conduction band edge and narrow band gap for sunlight absorption.

Among sulfide-based materials, sulfide solid solutions have attracted considerable attention because of their controllable band gap width and excellent performance for hydrogen evolution under visible light irradiation, such as $Zn_{1-x}Cd_xS$ [7], $ZnS-In_2S_3-Ag_2S$ [9], $(CuIn)_xZn_{2(1-x)}S_2$ [10], etc. Among these different solid solutions, the ternary solid solution $Mn_xCd_{1-x}S$ has recently been studied in hydrogen evolution under visible light irradiation. For example, Masato Machida, firstly synthesized $Mn_{1-x}Cd_xS$ with a high Mn content ($x \sim 0.1$) for hydrogen evolution from water under irradiation of visible light [11]. Liu synthesized $Mn_xCd_{1-x}S$ solid solution by a biomolecule-assisted hydrothermal method and investigated hydrogen evolution of different ratio of CdS to MnS [12]. However, the hydrogen evolution efficiency of pure $Mn_{1-x}Cd_xS$ is still low because of the rapid recombination of photogenerated electrons and holes. In order to improve the hydrogen evolution efficiency of $Mn_{1-x}Cd_xS$, some efforts have been done, such as doping (Ag-doped $Mn_{1-x}Cd_xS$) and modifying with other semiconductor ($Mn_{0.8}Cd_{0.2}S/g-C_3N_4$ heterojunction) [13,14].

Among various strategies, co-catalyst modification is one of the most effective methods. Noble metals are proved to be effective co-catalysts for hydrogen evolution, however, high cost and low reserve of noble metals limit their practical applications [15]. In recent years, earth abundant Ni-based co-catalysts have attracted

* Corresponding authors.

E-mail addresses: pengwangicm@sdu.edu.cn (P. Wang), bbhuang@sdu.edu.cn (B. Huang).

much attention. For example, Hong reported loading of 1.1 wt% NiS on C_3N_4 as a co-catalyst can enhance the H_2 evolution by about 250 times compared with the native C_3N_4 [16]. Yu synthesized NiS/ $Zn_xCd_{1-x}S$ /reduced graphene oxide (RGO) ternary composite photocatalysts with high photocatalytic H_2 evolution efficiency under simulated solar irradiation [17]. Zhang synthesized highly active NiS/CdS photocatalysts with a high quantum efficiency of 51.3% measured at 420 nm from lactic acid sacrificial solution [18].

In this work, we synthesized highly efficient and noble metal-free NiS modified $Mn_xCd_{1-x}S$ nanocomposites for the first time with enhanced photocatalytic activity for hydrogen evolution under visible light irradiation. $Mn_xCd_{1-x}S$ solid solutions are synthesized with the assistance of L-cystine as the S source via a facile hydrothermal route, and $Mn_{0.5}Cd_{0.5}S$ exhibits the highest photocatalytic activity. NiS modified $Mn_{0.5}Cd_{0.5}S$ is synthesized through a simple direct in situ precipitation process. The characteristics of the NiS/ $Mn_{0.5}Cd_{0.5}S$ nanocomposites with various amounts of NiS were analyzed. The results demonstrated that the photocatalytic hydrogen evolution of $Mn_{0.5}Cd_{0.5}S$ was significantly enhanced by loading NiS nanoparticles and exhibited good stability. The effects of NiS content on the photocatalytic activity, light absorption, charge separation were investigated in detail. The possible enhanced photocatalytic hydrogen evolution mechanism is also discussed.

2. Experimental section

2.1. Materials

Manganese acetate tetrahydrate ($Mn(CH_3COO)_2 \cdot 4H_2O$), cadmium acetate dihydrate ($Cd(CH_3COO)_2 \cdot 2H_2O$), L-cystine ($C_6H_{12}N_2O_4S_2$), sodium hydroxide (NaOH), nickel nitrate hexahydrate ($Ni(NO_3)_2 \cdot 6H_2O$), sodium sulfide nonahydrate ($Na_2S \cdot 9H_2O$) and sodium sulfite (Na_2SO_3) were analytic reagents and were used without further purification.

2.2. Synthesis of $Mn_xCd_{1-x}S$ solid solutions

In a typical procedure, $Mn(CH_3COO)_2 \cdot 4H_2O$ (2 x mmol) and $Cd(CH_3COO)_2 \cdot 2H_2O$ (2–2 x mmol) were added into 35 mL deionized water with constant stirring, marked as solution A. 6 mmol L-cystine was dissolved into another 35 mL deionized water and the pH value was adjusted to 10.5 using 6 mol/L NaOH, marked as solution B. After dissolving, solution A was slowly added to solution B to form a milky suspension. After stirring for 30 min, the mixture was transferred into a Teflon-lined autoclave with a capacity of 100 mL and maintained at 130 °C for 10 h. After cooling down to room temperature naturally, the product was obtained by filtering and washed with ethanol and deionized water alternately for three times and then dried at 60 °C for 6 h.

2.3. In situ synthesis of NiS modified $Mn_{0.5}Cd_{0.5}S$ nanocomposites

The prepared $Mn_{0.5}Cd_{0.5}S$ sample (0.15 g) was dispersed into 80 mL deionized water by sonication for 10 min, and then a given volume of 0.05 mol/L $Ni(NO_3)_2$ solution was added into the above solution. After stirring for 30 min at room temperature, Ni^{2+} ion absorbed on the surface of $Mn_{0.5}Cd_{0.5}S$. And then, excess Na_2S solution was dropped and continued to stir for another 10 min. The obtained products were filtered, washed with ethanol and deionized water for three times, respectively. Finally the products were dried at 60 °C for 6 h. The weight ratios of NiS to ($Mn_{0.5}Cd_{0.5}S + NiS$) were 0.1, 0.3, 0.5, 1.0 and 3.0 wt%. The final products were marked as 0.1 wt% NiS/ $Mn_{0.5}Cd_{0.5}S$, 0.3 wt% NiS/ $Mn_{0.5}Cd_{0.5}S$, 0.5 wt% NiS/ $Mn_{0.5}Cd_{0.5}S$, 1.0 wt% NiS/ $Mn_{0.5}Cd_{0.5}S$

and 3.0 wt% NiS/ $Mn_{0.5}Cd_{0.5}S$, respectively. Pt was loaded on $Mn_{0.5}Cd_{0.5}S$ by in situ photo-reduction using H_2PtCl_6 as a Pt source.

2.4. Material characterization

Crystal structures of as-obtained products were characterized by X-ray powder diffraction recorded on a Bruker AXS D8 diffractometer using Cu K α radiation. The Diffuse Reflectance Spectroscopy (DRS) of the products were recorded in the range from 200 to 800 nm using Shimadzu UV 2550 spectrophotometer equipped with an integrating sphere, using 100% $BaSO_4$ as a reflectance standard. Morphologies and microstructures of the products were characterized by scanning electron microscopy (Hitachi S-4800) equipped with an Energy Dispersive Spectrometer (EDS) and transmission electron microscopy (JEOL JEM-2100F). X-ray Photoelectron Spectroscopy (XPS) measurement was performed using a Thermo Fisher Scientific Escalab 250 spectrometer with monochromatized Al K α excitation, and C $1s$ (284.6 eV) was used to calibrate the peak positions of various elements. The PL spectra were carried out on a Hitachi F-4500 fluorescence spectrophotometer at room temperature and obtained with excitation wavelength at 330 nm. The time resolved fluorescence spectra were recorded at 520 nm with 377.8 nm excitation at room temperature by Edinburgh FLS920 PL, decay curves were fitted by using a biexponential decay function to obtain deconvolution of the instrument response function.

2.5. Photocatalytic H_2 evolution experiment

The typical photocatalytic H_2 evolution experiments were conducted in a 250 mL Pyrex flask keeping at room temperature (25 °C) with cooling water and atmospheric pressure, and the openings of the flask were sealed with silicone rubber stoppers. A 300 W Xe-lamp (CEL-HXF300, Beijing CEAULight, China) with a 420 nm cut-off filter was used as a visible light source for the photocatalytic experiment. 50 mg of NiS/ $Mn_{0.5}Cd_{0.5}S$ photocatalyst was well dispersed with ultrasound and constant stirring in a 100 mL mixed solution containing 0.1 mol/L Na_2S and 0.1 mol/L Na_2SO_3 . Before irradiation, the system was bubbled with argon for 30 min to remove oxygen in the reaction system. 50 μ L of gas was intermittently sampled from the reaction system, and the amount of hydrogen was analyzed by gas chromatograph (GC-7806, Shiweipx, Beijing, TCD with argon as a carrier gas and 5 Å molecular sieve column). The cycling photocatalytic test was performed to investigate the photocatalytic stability of NiS/ $Mn_{0.5}Cd_{0.5}S$ nanocomposite. After every 3 h irradiation, H_2 produced in the reaction system was evacuated by bubbling with argon and then run for another 3 h. After six cycles, the photocatalyst was recycled by centrifugation and re-dispersed in new solution. The apparent quantum efficiency (AQE) for H_2 evolution was measured under the same photocatalytic reaction conditions except a band pass interference filter of 420 nm (center wavelength 420 nm, band width 20 nm). The average intensity of irradiation was measured as 18.0 mW/cm 2 (PL-MW2000 spectroradiometer, PerfectLight, China) and the irradiation area was 28.26 cm 2 . The following equation was used to calculate the QE:

$$QE = \frac{2 \times \text{the number of evolved hydrogen molecules}}{\text{the number of incident photons}} \times 100\%$$

3. Results and discussion

3.1. XRD analysis of $Mn_xCd_{1-x}S$ and NiS/ $Mn_{0.5}Cd_{0.5}S$ nanocomposites

The phase structures of $Mn_xCd_{1-x}S$ and NiS/ $Mn_{0.5}Cd_{0.5}S$ nanocomposites were determined by X-ray diffraction. Fig. 1a

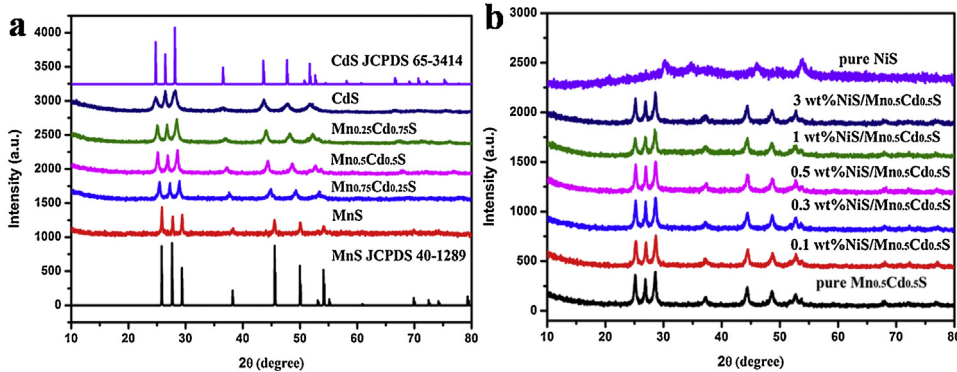


Fig. 1. (a) XRD patterns of the as-prepared $Mn_xCd_{1-x}S$ ($x=0, 0.25, 0.5, 0.75$ and 1) solid solutions, (b) XRD patterns of the as-prepared $NiS/Mn_{0.5}Cd_{0.5}S$ nanocomposites with different weight ratios of NiS .

shows XRD patterns of the as-prepared $Mn_xCd_{1-x}S$ ($x=0, 0.25, 0.5, 0.75$ and 1) solid solutions, together with the standard diffraction patterns of hexagonal wurtzite MnS (JCPDS Card No. 40-1289) and CdS (JCPDS Card No. 65-3414). All products exhibit similar diffraction patterns, with increasing Cd content in the $Mn_xCd_{1-x}S$ solid solution, the diffraction peaks exhibited an obvious shift to a lower angle from hexagonal wurtzite MnS (JCPDS Card No. 40-1289) to hexagonal CdS (JCPDS Card No. 65-3414). This implies that Cd^{2+} with larger ionic radius (0.97 \AA) than Mn^{2+} (0.46 \AA) incorporates into the lattice of the MnS crystal and increases the fringe lattice distance to form $Mn_xCd_{1-x}S$ solid solution. The precise stoichiometric ratios of $Mn_xCd_{1-x}S$ nanocomposites are $Mn_{0.24}Cd_{0.76}S$, $Mn_{0.47}Cd_{0.53}S$ and $Mn_{0.74}Cd_{0.26}S$, respectively. The detailed information can be seen in supporting Fig. S2. Fig. 1b shows XRD patterns of the as-prepared $NiS/Mn_{0.5}Cd_{0.5}S$ nanocomposites with different weight ratios of NiS, the diffraction peaks of pure NiS can be indexed to JCPDS 77-1624. However, no obvious diffraction peaks of NiS can be observed due to the low content and high dispersion.

3.2. Optical absorption of $Mn_xCd_{1-x}S$ and $NiS/Mn_{0.5}Cd_{0.5}S$ nanocomposites

The UV-vis diffuse reflectance spectra (DRS) of $Mn_xCd_{1-x}S$ were shown in Fig. 2a, absorption edge of the as-synthesized MnS locates at around 380 nm ($E_g=3.27\text{ eV}$), the absorption band has fluctuation in visible light region, which is probably associated with internal transitions in partly occupied 3d states of Mn and bulk defects in crystals [12,19]. With increasing of Cd content in $Mn_xCd_{1-x}S$ solid solutions, there are an obvious red shift of the absorption edges and E_g are 3.27 eV , 2.44 eV , 2.29 eV , 2.23 eV and 2.19 eV , respectively. The result also proves that the products are not simple mixtures of MnS and CdS, but $Mn_xCd_{1-x}S$ solid solutions. Fig. 2b shows the UV-vis diffuse reflectance spectra (DRS) of $NiS/Mn_{0.5}Cd_{0.5}S$ nanocomposites and pure NiS, the absorption edge of $Mn_{0.5}Cd_{0.5}S$ is not shifted, but the absorption bands are enhanced in visible light region after 540 nm with increasing NiS contents. The result indicates Ni^{2+} ions are not doped into $Mn_{0.5}Cd_{0.5}S$ but form NiS on the surface of $Mn_{0.5}Cd_{0.5}S$.

3.3. SEM and TEM analysis of $NiS/Mn_{0.5}Cd_{0.5}S$ nanocomposites

The surface morphologies of $NiS/Mn_{0.5}Cd_{0.5}S$ nanocomposite were investigated by SEM. From Fig. 3a, $NiS/Mn_{0.5}Cd_{0.5}S$ nanocomposite is constructed by small nanoparticles with an average particle size of 60 nm , which has no obvious change relative to $Mn_{0.5}Cd_{0.5}S$ in supporting Fig. S1c, for the reason of low content and high dispersion of NiS. In order to get more information on microstructures of $NiS/Mn_{0.5}Cd_{0.5}S$ nanocomposite, TEM and

HRTEM images were taken. Fig. 3b also shows the average particle size of $NiS/Mn_{0.5}Cd_{0.5}S$ nanocomposite is 60 nm , which is consistent with the SEM result. In Fig. 3c, two different kinds of lattice fringes are clearly observed. The main lattice fringes with a spacing of 0.336 nm match well with the spacing of the (002) crystal plane of $Mn_{0.5}Cd_{0.5}S$, the lattice fringes with a spacing of 0.198 nm match well with the spacing of the (102) crystal plane of NiS [20], further confirming the presence of NiS. Small NiS nanoparticles are well deposited and tightly contact with $Mn_{0.5}Cd_{0.5}S$, which is benefit for charge transfer between $Mn_{0.5}Cd_{0.5}S$ and NiS. EDS spectrum (Fig. 3d) further confirms the presence of Mn, Cd, S and Ni elements and detailed information about the content of Mn, Cd, S and Ni can be seen in supporting Fig. S3.

3.4. XPS analysis

So as to further study the surface chemical status and chemical compositions of $NiS/Mn_{0.5}Cd_{0.5}S$ nanocomposites, X-ray photo-electron spectrum analysis was carried out. Seen from Fig. 4a, Ni, Mn, Cd and S elements can be detected obviously which is in good agreement with the EDS result. The corresponding high resolution XPS spectra of Mn, Cd, Ni and S are shown in Fig. 4b–e. Mn 2p spectrum (Fig. 4b) displays two strong peaks at 652.2 eV and 641.3 eV corresponding to $2p_{1/2}$ and $2p_{3/2}$ of Mn^{2+} in $NiS/Mn_{0.5}Cd_{0.5}S$ nanocomposite, respectively. Cd 3d spectrum (Fig. 4c) displays two strong peaks at 411.4 eV and 404.8 eV corresponding to $3d_{3/2}$ and $3d_{5/2}$ of Cd^{2+} in $NiS/Mn_{0.5}Cd_{0.5}S$ nanocomposite, respectively. In Fig. 4c, binding energy of Ni 2p's peak is found at 856.6 eV , which corresponds with that of NiS. The S 2p peaks located at 162.3 eV and 161.1 eV are in accordance with the $2p_{1/2}$ and $2p_{3/2}$ of S^{2-} in $NiS/Mn_{0.5}Cd_{0.5}S$ nanocomposite. The binding energy peaks of Ni, Mn, Cd and S are consistent with previous reports [12,14,20,21]. XPS result further proves that NiS is deposited on the surface of $Mn_{0.5}Cd_{0.5}S$ solid solution.

3.5. Photocatalytic H_2 evolution activity and stability

Photocatalytic H_2 evolution activities of all products were evaluated under visible light irradiation ($\lambda \geq 420\text{ nm}$) using Na_2S (0.1 mol/L) and Na_2SO_3 (0.1 mol/L) as sacrificial reagents, just as shown in Fig. 5. No H_2 evolution was detected without light irradiation or photocatalyst, indicating that H_2 was produced only by photocatalytic reactions. In Fig. 5a, $Mn_{0.5}Cd_{0.5}S$ exhibits the highest H_2 evolution rate of $22.53\text{ }\mu\text{mol/h}$ among $Mn_xCd_{1-x}S$ ($x=0, 0.25, 0.5, 0.75, 1$) solid solutions. In Fig. 5b, after loading NiS as co-catalyst, H_2 evolution performance of $Mn_{0.5}Cd_{0.5}S$ gets enhanced a lot, demonstrating that NiS is an effective co-catalyst for $Mn_{0.5}Cd_{0.5}S$. The photocatalytic H_2 evolution of $Mn_{0.5}Cd_{0.5}S$

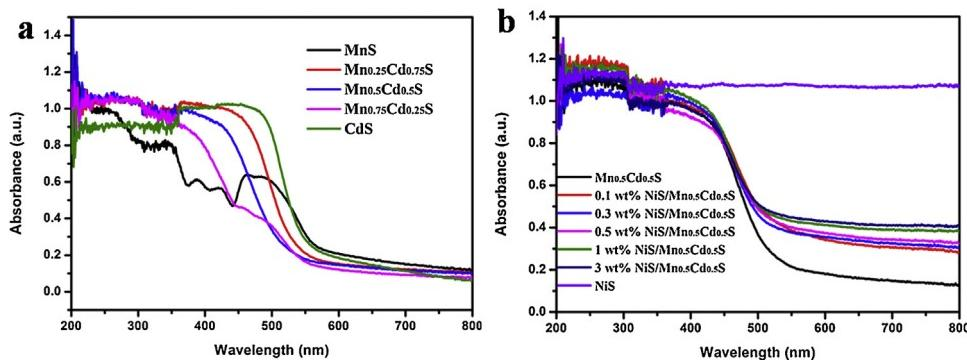


Fig. 2. (a) The UV-vis diffuse reflectance spectra of Mn_xCd_{1-x}S ($x=0, 0.25, 0.5, 0.75$ and 1) solid solutions, (b) the UV-vis diffuse reflectance spectra of NiS/Mn_{0.5}Cd_{0.5}S nanocomposites and pure NiS.

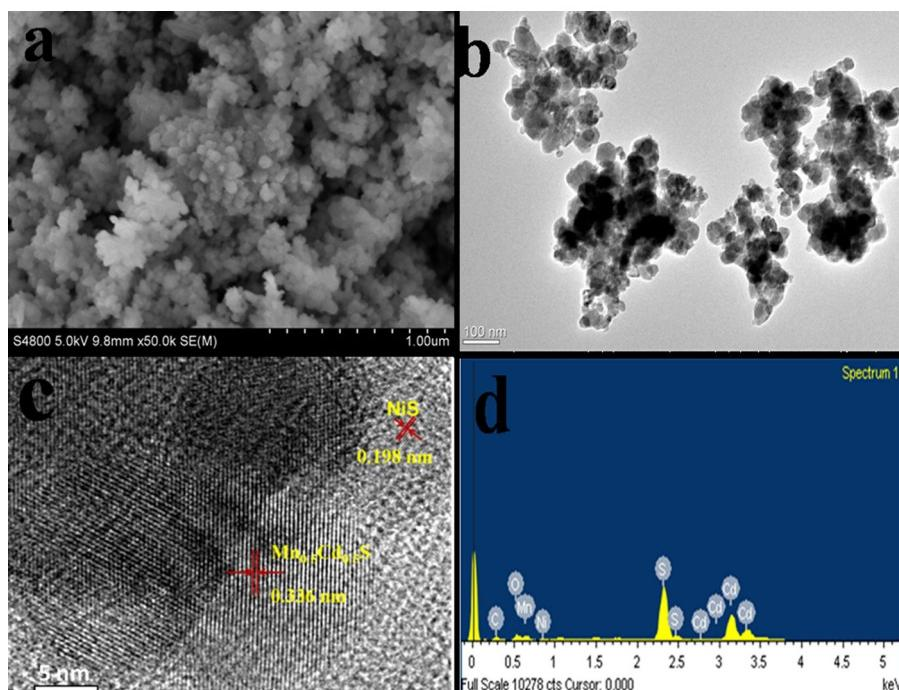


Fig. 3. (a) SEM image of 0.5 wt% NiS/Mn_{0.5}Cd_{0.5}S nanocomposite, (b) TEM image of 0.5 wt% NiS/Mn_{0.5}Cd_{0.5}S nanocomposite, (c) HRTEM image of 0.5 wt% NiS/Mn_{0.5}Cd_{0.5}S nanocomposite, (d) EDS spectrum of 0.5 wt% NiS/Mn_{0.5}Cd_{0.5}S nanocomposite.

increases from 301.7 to 419.3 μmol/h, as the content of NiS increases from 0.1 to 0.3 wt%. When the content of NiS further increases, the photocatalytic H₂ evolution of Mn_{0.5}Cd_{0.5}S decreases. The optimal NiS content is 0.3 wt% with the highest H₂ evolution rate of 419.3 μmol/h which is about 3.1 times than that of 1.0 wt% Pt/Mn_{0.5}Cd_{0.5}S nanocomposite which has the optimal H₂ evolution activity among Pt/Mn_{0.5}Cd_{0.5}S nanocomposites (part 5 in the Supporting information). The overmuch content of NiS can act as recombination centers of photon-generated carriers and reduce the light absorption of Mn_{0.5}Cd_{0.5}S.

Stability and reusability are significant for catalysts in practical applications. In order to evaluate the stability and reusability of 0.3 wt% NiS/Mn_{0.5}Cd_{0.5}S nanocomposite, the cycling photocatalytic test was performed for ten times under the same condition (Fig. 6). And the result revealed that photocatalytic H₂ evolution of 0.3 wt% NiS/Mn_{0.5}Cd_{0.5}S photocatalyst kept good stability during the first five cycles, with further increase of cycling times, the photocatalytic H₂ evolution activity showed a bit decrease. After ten cycles, the amount of H₂ evolution is also about 72% relative to the first cycle which is still more than that of 1.0 wt% Pt/Mn_{0.5}Cd_{0.5}S.

The results indicate that NiS/Mn_{0.5}Cd_{0.5}S photocatalyst is stable for photocatalytic H₂ evolution and NiS is an efficient co-catalyst to replace noble metal.

3.6. PL and time-resolved PL spectrum

For the purpose of studying charge migration, recombination and transfer behavior in NiS/Mn_{0.5}Cd_{0.5}S, photoluminescence (PL) emission spectrum was employed [21,22]. PL spectra of Mn_{0.5}Cd_{0.5}S and 0.3 wt% NiS/Mn_{0.5}Cd_{0.5}S are presented in Fig. 7a with an excitation wavelength of 330 nm. As shown in Fig. 7a, pure Mn_{0.5}Cd_{0.5}S displays higher PL emission intensity, indicating that photo-generated carriers recombine quickly. When loading 0.3 wt% NiS on Mn_{0.5}Cd_{0.5}S, PL emission intensity gets an obvious decrease. This phenomenon illustrating that the charge recombination can be efficiently suppressed after loading NiS on Mn_{0.5}Cd_{0.5}S, leading to lower PL intensity.

Charge carrier lifetime plays an important role in photocatalytic reactions, the longer charge carrier lifetime lasts, more photo-generated electrons and holes participate in photocatalytic

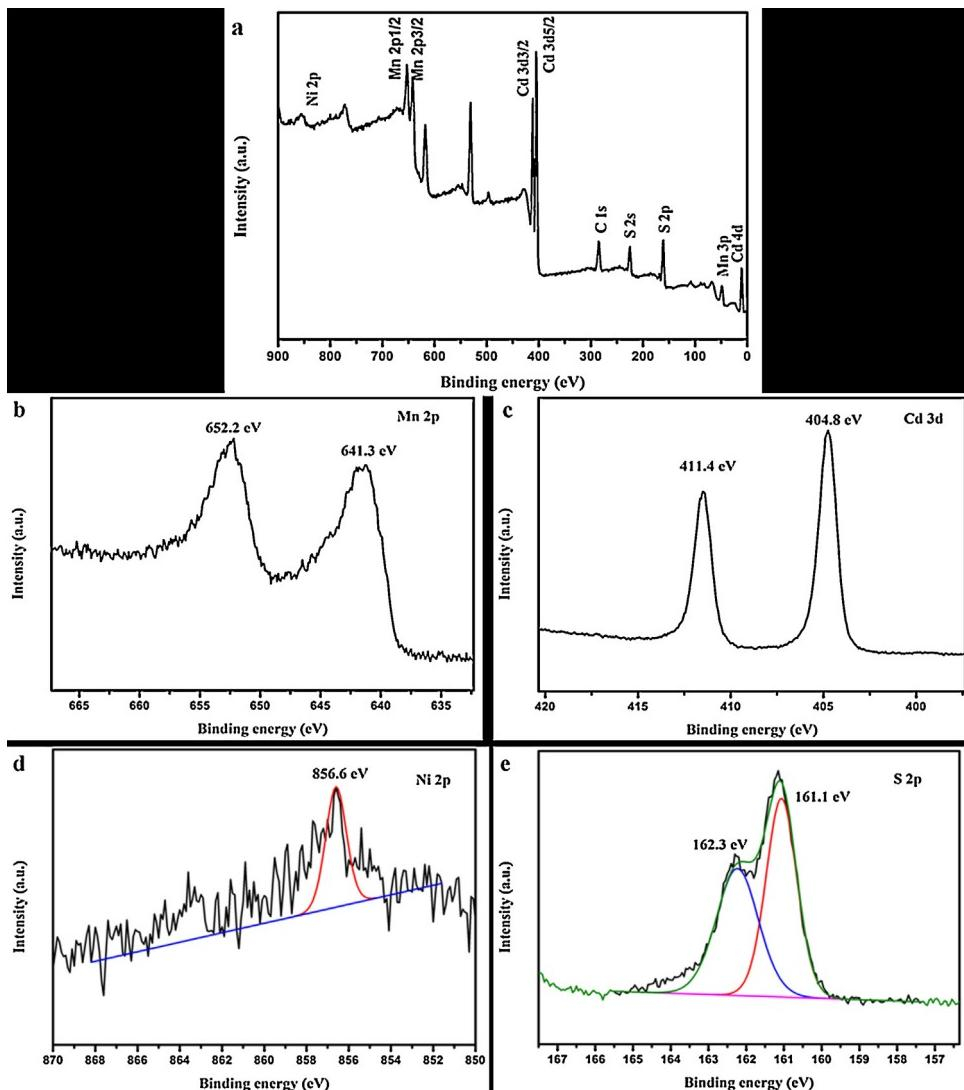


Fig. 4. XPS spectra of 0.5 wt% NiS/Mn_{0.5}Cd_{0.5}S: (a) the wide-scan XPS spectrum of 0.5 wt% NiS/Mn_{0.5}Cd_{0.5}S, (b) the high resolution XPS spectrum of Mn, (c) the high resolution XPS spectrum of Cd, (d) the high resolution XPS spectrum of Ni, (e) the high resolution XPS spectrum of S.

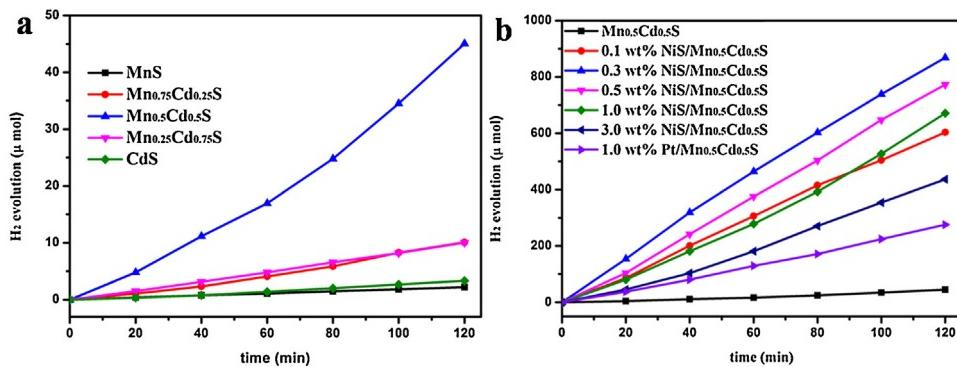


Fig. 5. (a) Comparison of photocatalytic H₂ evolution activities of Mn_xCd_{1-x}S solid solutions ($x = 0, 0.25, 0.5, 0.75, 1$) under visible light irradiation ($\lambda \geq 420$ nm), (b) Comparison of photocatalytic H₂ evolution activities of Mn_xCd_{1-x}S with different loading of NiS under visible light irradiation ($\lambda \geq 420$ nm).

reactions [23]. The lifetime of charge carriers in Mn_{0.5}Cd_{0.5}S and 0.3 wt% NiS/Mn_{0.5}Cd_{0.5}S were examined by time-resolved PL spectrum, as shown in Fig. 7b. The average lifetime was calculated by using the following relation: $\tau_{av} = a_1\tau_1 + a_2\tau_2 + a_3\tau_3$, (τ_1 , τ_2 and τ_3 are the lifetime, a_1 , a_2 and a_3 are normalized pre-exponential factors) [24]. The average lifetime of Mn_{0.5}Cd_{0.5}S and 0.3 wt%

NiS/Mn_{0.5}Cd_{0.5}S are 2.27 ns and 3.06 ns, respectively. When loading 0.3 wt% NiS on Mn_{0.5}Cd_{0.5}S, the lifetime of charge carriers gets increased. The charge recombination is efficiently suppressed after loading NiS on Mn_{0.5}Cd_{0.5}S, resulting in higher photocatalytic activity.

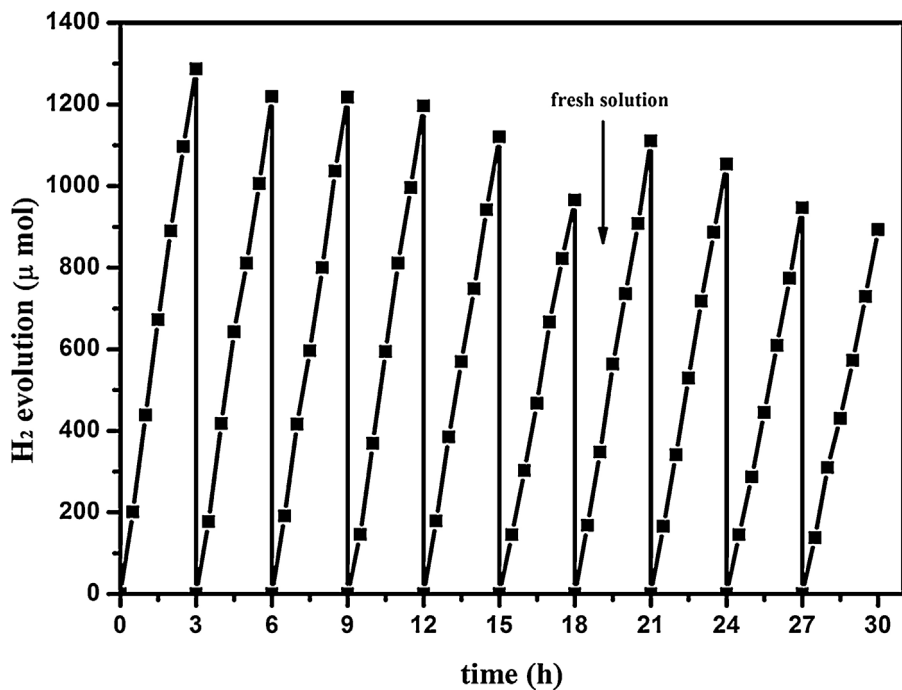


Fig. 6. Cycling photocatalytic H₂ evolution test of 0.3 wt% NiS/Mn_{0.5}Cd_{0.5}S nanocomposite.

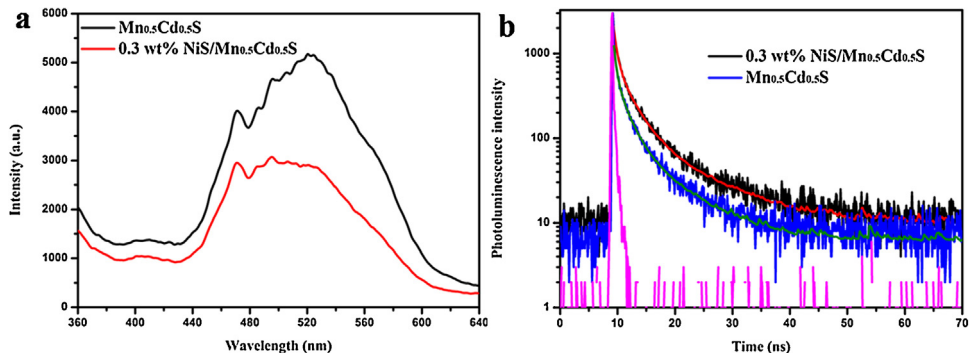


Fig. 7. (a) PL spectra of Mn_{0.5}Cd_{0.5}S and 0.3 wt% NiS/Mn_{0.5}Cd_{0.5}S ($\lambda_{\text{exc}} = 330 \text{ nm}$). (b) Time-resolved PL spectra for Mn_{0.5}Cd_{0.5}S and 0.3 wt% NiS/Mn_{0.5}Cd_{0.5}S detected at 520 nm, the excitation source is a 377.8 nm laser. The pink curve represents the instrument response time.

3.7. Possible mechanisms of photocatalytic H₂ evolution

On the basis of all the above results, possible photocatalytic H₂ evolution and photogenerated electrons and holes transfer mechanisms in NiS/Mn_{0.5}Cd_{0.5}S composite systems are shown in Fig. 8. Under visible light irradiation, Mn_{0.5}Cd_{0.5}S absorbs photons giving rise to electrons and holes. Although the CB position of Mn_{0.5}Cd_{0.5}S is more negative (−0.8 eV) than the reduction potential of H⁺/H₂, the rapid recombination of electrons and holes in Mn_{0.5}Cd_{0.5}S leads to negligible H₂ evolution rate. After loading NiS as co-catalyst, from the HRTEM, it can be seen that NiS nanoparticles can form intimate contact with Mn_{0.5}Cd_{0.5}S. Due to the intimate contact, the photogenerated electrons in the CB of Mn_{0.5}Cd_{0.5}S can be easily transferred to the surface NiS nanoparticles. The electrons are trapped by NiS to form the intermediate HNiS by absorption-reduction of H⁺, and H₂ can be released by the intermediate HNiS with reduction of another H⁺ [18,25]. The formation of hydride-NiS intermediate in many hydrotreating processes has been experimentally and computationally reported [26–28]. Meanwhile, the photogenerated holes in the VB of Mn_{0.5}Cd_{0.5}S can be consumed by the sacrificial reagents (Na₂S and Na₂SO₃). Consequently, the

photogenerated electrons and holes can be effectively separated, the photocatalytic H₂ evolution activity gets promoted for NiS co-catalyst modified Mn_{0.5}Cd_{0.5}S nanocomposites.

4. Conclusions

In summary, Mn_{0.5}Cd_{0.5}S exhibits the highest H₂ evolution rate among Mn_xCd_{1-x}S solid solutions. A series of NiS modified Mn_{0.5}Cd_{0.5}S nanocomposites were synthesized via a simple in situ precipitation method. The results reveal NiS is an effective and stable co-catalyst to improve photocatalytic H₂ evolution activity of Mn_{0.5}Cd_{0.5}S. The optimal loading content of NiS is 0.3 wt% for Mn_{0.5}Cd_{0.5}S giving a photocatalytic H₂ evolution rate of 419.3 μmol/h with an apparent quantum efficiency (QE) of 5.21% measured at 420 nm, which is nearly 18.6 and 3.1 times than that of pure Mn_{0.5}Cd_{0.5}S and 1.0 wt% Pt/Mn_{0.5}Cd_{0.5}S. During photocatalytic H₂ evolution under visible light irradiation, NiS acts as electron-trapping center and high active site to prevent charge recombination, and improve the photocatalytic H₂ evolution activity. This work demonstrates that low cost and earth-abundant NiS

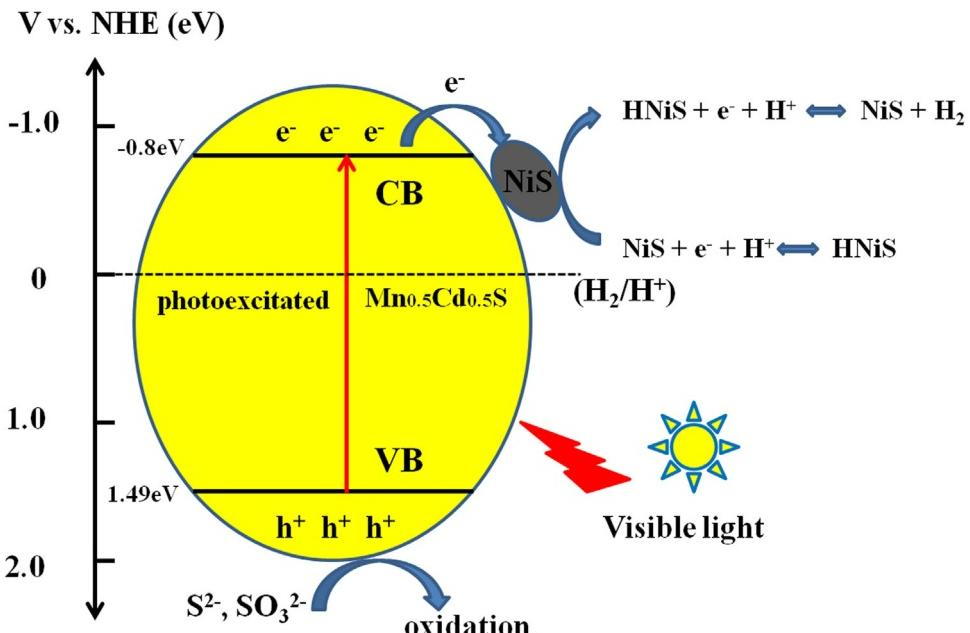


Fig. 8. The possible photocatalytic H_2 evolution and photogenerated electrons and holes transfer mechanism in $\text{NiS}/\text{Mn}_{0.5}\text{Cd}_{0.5}\text{S}$ composite systems under visible light irradiation.

can replace noble metal Pt as a highly efficient co-catalyst in photocatalytic H_2 evolution.

Acknowledgements

This work was financially supported by a research Grant from the National Basic Research Program of China (973 program, No. 2013CB632401), the National Natural Science Foundation of China (Nos. 21333006, 21573135, 11374190, 51002091, and 21007031), The Recruitment Program of Global Experts, China, Taishan Scholar Foundation of Shandong Province, China, and Shandong Province Natural Science Foundation (ZR2014JL008).

Appendix A. Supplementary data

Supplementary data associated with this article can be found, in the online version, at <http://dx.doi.org/10.1016/j.apcatb.2016.10.040>.

References

- [1] R.D. Crighton, R.R. Davda, J.A. Dumesic, *Nature* 418 (2002) 964–967.
- [2] H. Tong, S.X. Ouyang, Y.P. Bi, N. Umezawa, M. Oshikiri, J.H. Ye, *Adv. Mater.* 24 (2012) 229–251.
- [3] A. Fujishima, K. Honda, *Nature* 238 (1972) 37–38.
- [4] L.J. Zhang, T.F. Jiang, S. Li, Y.C. Lu, L.L. Wang, X.Q. Zhang, D.J. Wang, T.F. Xie, *Dalton Trans.* 42 (2013) 12998.
- [5] J.G. Yu, Y. Hai, B. Cheng, *J. Chem. Phys. C* 115 (2011) 4953–4958.
- [6] S.N. Guo, Y.L. Min, J.C. Fan, Q.J. Xu, *ACS Appl. Mater. Interfaces* 8 (5) (2016) 2928–2934.
- [7] Q. Li, H. Meng, P. Zhou, Y.Q. Zheng, J. Wang, J.G. Yu, J.R. Gong, *ACS Catal.* 3 (2013) 882–889.
- [8] Ryu Abe, Masanobu Higashi, Kazunari Domen, *J. Am. Chem. Soc.* 132 (34) (2010) 11828–11829.
- [9] Y.X. Li, G. Chen, C. Zhou, J.X. Sun, *Chem. Commun.* (2009) 2020–2022.
- [10] M. Xu, J. Zai, Y. Yuan, X. Qian, *J. Mater. Chem.* 22 (2012) 23929.
- [11] K. Ikeue, S. Shiiba, M. Machida, *Chem. Mater.* 22 (2010) 743–745.
- [12] M.Y. Liu, L.Q. Zhang, X.X. He, B. Zhang, H.F. Song, S.N. Li, W.S. You, *J. Mater. Chem. A* 2 (2014) 4619–4626.
- [13] K. Ikeue, Y. Shimura, M. Machida, *Appl. Catal. B: Environ.* 123–124 (2012) 84–88.
- [14] H. Liu, Z.Z. Xu, Z. Zhang, D. Ao, *Appl. Catal. A: Gen.* 518 (2016) 150–157.
- [15] Z.P. Yan, Z.J. Sun, X. Liu, H.X. Jia, P.W. Du, *Nanoscale* 8 (2016) 4748–4756.
- [16] J.D. Hong, Y.S. Wang, Y.B. Wang, W. Zhang, R. Xu, *ChemSusChem* 6 (2013) 2263–2268.
- [17] J. Zhang, L.F. Qi, J.R. Ran, J.G. Yu, S.Z. Qiao, *Adv. Energy Mater.* 4 (2014) 1301925.
- [18] W. Zhang, Y.B. Wang, Z. Wang, Z.Y. Zhong, R. Xu, *Chem. Commun.* 46 (2010) 7631–7633.
- [19] M. Machida, S. Murakami, T. Kijima, S. Matsushima, M. Arai, *J. Phys. Chem. B* 105 (2001) 3289.
- [20] Z.H. Chen, P. Sun, B. Fan, Z.G. Zhang, X.M. Fang, *J. Phys. Chem. C* 118 (2014) 7801–7807.
- [21] Y.M. Zhong, J.L. Yuan, J.Q. Wen, X. Li, Y.H. Xu, W. Liu, S.S. Zhang, Y.P. Fang, *Dalton Trans.* 44 (2015) 18260.
- [22] X.L. Liu, W.J. Wang, Y.Y. Liu, B.B. Huang, Y. Dai, X.Y. Qin, Z.X. Yang, *RSC Adv.* 5 (2015) 55957.
- [23] G.Z. Wang, Q.L. Sun, Y.Y. Liu, B.B. Huang, Y. Dai, X.Y. Zhang, X.Y. Qin, *Chem. Eur. J.* 21 (2015) 2364–2367.
- [24] L. Zhang, B.Z. Tian, F. Chen, J.L. Zhang, *Int. J. Hydrogen Energy* 37 (2012) 17060–17067.
- [25] M. Breysse, E. Furimsky, S. Kasztelan, M. Lacroix, G. Perot, *Catal. Rev.* 44 (2002) 651–735.
- [26] M.Y. Sun, A.E. Nelson, J. Adjaye, *J. Catal.* 233 (2005) 411.
- [27] D.Y. Hwang, A.M. Mebel, *J. Phys. Chem. A* 106 (2002) 520.